Transverse magneto-optic Kerr effect and Imbert–Fedorov shift upon light reflection from a magnetic/non-magnetic bilayer: impact of misfit strain

2017 J. Opt. 19 015610

(http://iopscience.iop.org/2040-8986/19/1/015610)

J. Opt. **19** (2017) 015610 (10pp) doi:10.1088/2040-8986/19/1/015610

Transverse magneto-optic Kerr effect and Imbert–Fedorov shift upon light reflection from a magnetic/non-magnetic bilayer: impact of misfit strain

Yu S Dadoenkova[1,2,3], **F F L Bentivegna**[4], **N N Dadoenkova**[1,3] and **I L Lyubchanskii**[3]

[1] Ulyanovsk State University, Ulyanovsk 432017, Russian Federation
[2] Institute of Electronic and Information Systems, Novgorod State University, Veliky Novgorod 173003, Russian Federation
[3] Donetsk Physical & Technical Institute of the National Academy of Sciences of Ukraine, Donetsk 83114, Ukraine
[4] Lab-STICC (UMR 6285), CNRS, UBL, ENIB, 29238 Brest Cedex 3, France

E-mail: yulidad@gmail.com

Received 29 August 2016, revised 31 October 2016
Accepted for publication 15 November 2016
Published 13 December 2016

CrossMark

Abstract
We present a theoretical study of the influence of the misfit strain on the transverse magneto-optic Kerr effect (TMOKE) and the transverse shift (Imbert–Fedorov effect) experienced by a light beam reflected from the surface of a magnetic/non-magnetic bilayer. The bilayer consists of a magnetic, gyrotropic yttrium-iron garnet film epitaxially grown on a non-magnetic dielectric gadolinium-gallium garnet slab. We use Green's function method to calculate the reflection matrix in the presence of strain. It is shown that the mechanical strain present in the vicinity of the geometrical interface between the constituents of the bilayer can induce a non-negligible contribution to the TMOKE and the Imbert–Fedorov shift (IFS) for incidence angles close to those satisfying the half-wave condition for both layers, at which neither the TMOKE nor the transverse shift would appear in the absence of strain. We analyze the dependence of the IFS on the state of polarization of the incident beam, the thickness of both layers, and the direction of magnetization in the magnetic layer.

Keywords: beam shifts, Imbert–Fedorov effect, misfit strain, transverse magneto-optic Kerr effect

(Some figures may appear in colour only in the online journal)

1. Introduction

It is well known that upon reflection of a finite-size light beam from a planar surface the reflected beam can be shifted parallel and/or perpendicular to the incidence plane as compared to the predictions of geometric optics. The lateral shift of a reflected beam, parallel to the incidence plane, was observed experimentally for the first time in 1947 by Goos and Hänchen in the case of the total internal reflection at the interface between two dielectric media [1]. A beam shift perpendicular to the incidence plane, or transverse shift, was theoretically predicted by Fedorov in 1955 [2] and observed by Imbert in 1972 [3]. Since then, numerous theoretical and experimental works have been devoted to both Goos–Hänchen and Imbert–Fedorov effects, not only for total internal reflection of light [4], but also for partial reflection and transmission [5–8]. Beyond their fundamental interest, the Goos–Hänchen shift (GHS) and Imbert–Fedorov shift (IFS) of beams of different shapes [9] upon the reflection from, or the transmission through, virtually any type of surface, including in dielectric

[10], metallic [11], electro-optic [12, 13] or magneto-optic (MO) materials [14, 15], graphene [16], superconducting [17] and photonic crystals [18, 19], at the interface of dielectric and topological insulator [20], or in an anisotropic chiral medium [21], have become relevant to many technological domains [4].

A few recent examples of the many applications of the Goos–Hänchen and Imbert–Fedorov effects include the study of GHS and IFS at a surface coated with a single layer of graphene [22]; the investigation of surface plasmon resonance on the GHS and IFS upon reflection of terahertz waves is investigated in [16], where it is predicted that giant IFSs could be obtained and controlled with a voltage applied to a graphene-based metamaterial; the use of the IFS as a very sensitive way of determining the weak value of the polarization of a light beam upon propagation [7]; the thermal control of the Goos–Hänchen and Imbert–Fedorov effects in a prism-waveguide coupling system [23, 24]; the theoretical study of the IFS upon reflection of massless fermions in Weyl semimetals as a consequence of the wave-particle duality of such particles [25]; the control of the IFS via pump and driving fields [26]; or the spatial and angular IFSs at an air-magnetoplasma interface [27].

Upon reflection from an optical system, both the longitudinal and the transverse shifts depend on the properties of the incoming beam, i.e., its wavelength, beam waist, state of polarization and incidence angle. On the other hand, the material parameters of the optical system and the physical properties of its interfaces also affect the beam shifts. In particular, it is well known that the crystalline lattice misfit between neighboring materials produces elastic strain in the vicinity of interfaces in stratified structures [28, 29]. In turn, elastic strain gives rise to crystalline deformations near interfaces, which modifies the refractive indices via the photoelastic interaction and results in changes in the reflectivity and transmittivity of the optical system [30–34]. We recently investigated theoretically the GHS upon the reflection of light from the upper surface of a strained bilayer consisting of a magnetic slab of yttrium-iron garnet (YIG) epitaxially grown on a non-magnetic slab of gadolinium-gallium garnet (GGG) [35] in the transverse MO Kerr effect (TMOKE) geometry [36]. TMOKE results in a change of the intensity of light reflected from a magnetic material upon magnetization reversal and is thus widely used for the investigation of the magnetic properties of media, and can be applied to MO data storage [36]. The influence of misfit strain on TMOKE has been investigated experimentally [37, 38], but theoretical models have not been proposed so far. Similarly, it has been demonstrated that the magnitude of magneto-optical anisotropy in epitaxial hcp Co films is directly correlated with epitaxial strain [39]. It has also been shown that by inducing a pseudomagnetic field in graphene with the help of an applied strain field, one can achieve Faraday and Kerr rotation angles of $\pi/8$ and $\pi/4$, respectively, for suitable terahertz waves [40]. Furthermore, in [35] strain has been shown to induce noticeable GHSs at incidence angles satisfying the half-wave condition for both layers, where no shift would be observed otherwise.

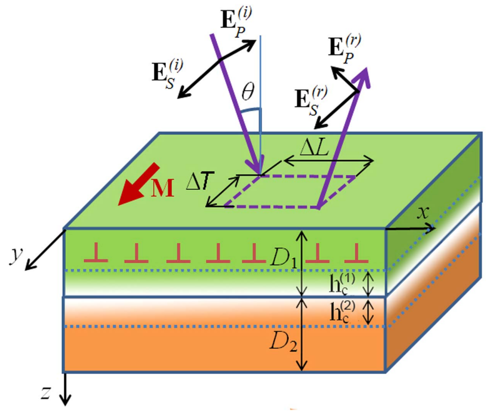

Figure 1. Geometry of the system: a magnetic film (thickness D_1) is epitaxially grown on a non-magnetic slab (thickness D_2). The thicknesses of the pseudomorphic regions on each side of the film/slab interface are $h_c^{(1)}$ and $h_c^{(2)}$. The magnetization M in the film is parallel to the y-axis. The s- and p-components of the incident (i) and reflected (r) electric fields of light are denoted $E_{s,p}^{(i,r)}$. The GHS (in the incidence plane) is ΔL, and the IFS (perpendicular to the incidence plane) is ΔT.

Thus, misfit strain can be expected to affect both TMOKE and the IFS in similar conditions. In this paper, we focus on a study of these effects upon reflection of light beam from the same structure as in [35], with a similar approach based on the Green's functions method. In section 2 we describe the geometry of the system and provide a succinct analysis of the contribution of elastic strain to the permittivity tensors of the materials on each side of the geometrical interface. In section 3, we show the results of numerical simulations of TMOKE and IFS in the aforementioned YIG/GGG bilayer, and discuss in particular the influence of elastic strain near their common geometrical interface, of the magnetization in the magnetic film, and of the thicknesses of the layers on the transverse shift. Finally we compare the influence of misfit strain on the GHS and IFS. In Conclusion we summarize our results.

2. Description of the system

Let us consider a monochromatic polarized wavepacket of angular frequency ω impinging in vacuum and under oblique incidence angle θ the upper surface of a bilayered structure consisting of a thin magnetic film of YIG (henceforth identified by index $\alpha = 1$) of thickness D_1 epitaxially grown on a non-magnetic dielectric GGG slab ($\alpha = 2$) of thickness D_2, as illustrated in figure 1. The geometric interface between the materials is parallel to the (xy) plane of a Cartesian system of coordinates, and (xz) is the incidence plane. The incident and reflected waves (denoted with superscripts (i) and (r), respectively) are elliptically polarized and can be decomposed into s- and p-components of electric field strengths $E_{s,p}^{(i,r)}$. We investigate the transverse MO configuration, in which the YIG film is magnetized along the y-axis, i.e., $\mathbf{M} = \pm M_S\ \hat{\mathbf{y}}$, where M_S is the saturation magnetization, and can thus give rise to TMOKE. The direction of magnetization can be reversed through the application of an external magnetic field.

The crystals of YIG and GGG have similar cubic crystal lattices and can easily be grown on top of each other, as their lattice constants a_1 and a_2, respectively, only slightly differ ($a_1 = 1.2376$ nm and $a_2 = 1.2400$ nm [41]). However, the lattice mismatch is enough to induce strain in the vicinity of their common interface. On each side of that interface, in a pseudomorphic region delimited with dotted lines in figure 1, the mechanical strain is homogeneous. The thicknesses of the pseudomorphic regions (called critical thicknesses) are denoted $h_c^{(1)}$ and $h_c^{(2)}$. When $D_1 > h_c^{(1)}$, so-called edge dislocations [29], indicated by symbols '⊥' in figure 1, appear above that region in the magnetic film, where they tend to compensate for misfit strain and minimize the total mechanical strain energy during epitaxial growth.

The modification of the relative permittivity tensor of the material due to strain on each side of the geometric interface can be written as:

$$\hat{\varepsilon}^{(\alpha)} = \hat{\varepsilon}^{(\alpha,0)} + \delta\hat{\varepsilon}^{(\alpha)} = \hat{\varepsilon}^{(\alpha,0)} + p_{ijkl}^{(\alpha)}\ u_{kl}^{(\alpha)},\ \ \alpha = (1,\ 2), \tag{1}$$

where $\hat{\varepsilon}^{(\alpha,0)}$ is the dielectric permittivity tensor of the strain-free material, and the second term $\delta\,\hat{\varepsilon}^{(\alpha)}$ describes the strain-induced contribution to its permittivity, where $u_{kl}^{(\alpha)}$ and $p_{ijkl}^{(\alpha)}$ are the elements of the strain tensor and the linear photo-elastic tensor of the material, respectively, and can be found in our recent paper [35].

In first approximation, the strain-dependent contributions to the permittivity tensors in each of the four regions of the bilayer are given by:

$$\begin{aligned}\delta\varepsilon_{xx}^{(\alpha)}(z) &= \delta\varepsilon_{yy}^{(\alpha)}(z) = u^{(\alpha)}(z)\\ &\times\left[p_{11}^{(\alpha)} + p_{12}^{(\alpha)}\left(1 - \frac{2\nu^{(\alpha)}}{1-\nu^{(\alpha)}}\right)\right],\\ \delta\varepsilon_{zz}^{(\alpha)}(z) &= u^{(\alpha)}(z)\left[2p_{12}^{(\alpha)} - p_{11}^{(\alpha)}\frac{2\nu^{(\alpha)}}{1-\nu^{(\alpha)}}\right],\end{aligned} \tag{2}$$

where the usual reduced matrix symbols for the representation of higher-rank tensors are used, i.e., $1 \equiv 11$, $2 \equiv 22$. In the pseudomorphic layer, strain is homogeneous, while in the regions of the bilayer further away from the interface, misfit dislocations in the film lead to a gradual reduction of the strain. This can be estimated to result in an exponential decrease of the strain tensor elements (whose contribution to the strain-dependent permittivity in equation (2) is given by functions $u^{(\alpha)}(z)$) with an increasing distance from the dislocation pileup plane [35, 42].

In the transverse MO configuration and in a linear MO approximation, the dielectric permittivity tensor of the unstrained magnetic slab writes

$$\hat{\varepsilon}^{(1,0)} = \begin{pmatrix} \varepsilon_1 & 0 & -\mathrm{i}f_e\, m_y \\ 0 & \varepsilon_1 & 0 \\ \mathrm{i}f_e\, m_y & 0 & \varepsilon_1 \end{pmatrix}, \tag{3}$$

where time dependence of the fields is taken as exp(–iωt), f_e is the gyroelectric coefficient of the magnetic film and $m_y = M_y/M_S$ is its reduced magnetization [36]. The permittivity of the non-magnetic slab can simply be written as $\varepsilon_{ij}^{(2,0)} = \varepsilon_2\,\delta_{ij}$. Furthermore, we also neglect a potential magnetic gyrotropy of the magnetic slab, i.e., a dependence of its permeability upon magnetization. In the near-infrared domain, the permeability of both materials can be taken as that of the vacuum.

Taking strain-dependent perturbations of the permittivity (equation (2)) into account, the wave equation in the inhomogeneous structure can be written as:

$$\mathbf{grad}(\mathrm{div}\,\boldsymbol{E}) - \boldsymbol{\Delta E} - k_0^2\,\hat{\varepsilon}^{(0)}\boldsymbol{E} = k_0^2\,\delta\hat{\varepsilon}(z)\,\boldsymbol{E}, \tag{4}$$

and its solutions can be obtained using the Green's functions approach, as described in detail in [35].

Given the O_h symmetry of both YIG and GGG crystals and the choice of a transverse MO configuration in the magnetic layer, the s- and p-states of polarization are eigenmodes of the structure. Solving equation (4) and accounting for the boundary conditions, one can connect the complex amplitudes of the s- and p-components $E_{s,\,p}^{(r)}$ of the reflected field to those of the incident field $E_{s,\,p}^{(i)}$ as:

$$\begin{pmatrix} E_s^{(r)} \\ E_p^{(r)} \end{pmatrix} = \begin{pmatrix} \mathfrak{R}_s & 0 \\ 0 & \mathfrak{R}_p \end{pmatrix}\begin{pmatrix} E_s^{(i)} \\ E_p^{(i)} \end{pmatrix}, \tag{5}$$

where the complex reflection coefficients $\mathfrak{R}_s$ and $\mathfrak{R}_p$ of the s- and p-components of the electromagnetic radiation can be written as:

$$\mathfrak{R}_{s,p} = \mathfrak{R}_{s,p}^{(0)} + \mathfrak{R}_{s,p}^{(\mathrm{str})}, \tag{6}$$

i.e., as the sum of the reflection coefficients $\mathfrak{R}_{s,p}^{(0)}$ of the unstrained structure and strain-induced first-order corrections $\mathfrak{R}_{s,\,p}^{(\mathrm{str})}$. Thus, as follows from equations (2)–(4), misfit strain modifies the reflection coefficients via the photo-elastic corrections it induces in the dielectric permittivity tensors of the materials constituting the bilayer.

As a result, misfit strain exerts an influence on both the TMOKE and the transverse shift experienced by the reflected beam. Indeed, the reflection matrix is sufficient to define and calculate both the relative change of reflected light intensity $I_{s,p}^{(r)}\ (m_y) \sim |\ \mathfrak{R}_{s,p}(m_y)|^2$ upon magnetization reversal characteristic of TMOKE and the IFS experienced by the beam. For each eigenmode, TMOKE is characterized by [36]:

$$\delta_{\mathrm{TMOKE}} = \frac{I^{(r)}(m_y = +1) - I^{(r)}(m_y = -1)}{I^{(r)}(m_y = 0)}, \tag{7}$$

and is thus directly related to the strain-modified reflection coefficients. So is the transverse IFS. As a rule, when a monochromatic Gaussian wavepacket of elliptical polarization impinges on the uppermost surface of an optical structure, its reflection undergoes a non-negligible lateral GHS in the plane of incidence (in our case, along the x-axis) and transverse IFS perpendicular to the plane of incidence (i.e., along the y-axis), denoted ΔL and ΔT, respectively, in figure 1. The GHS in the structure under consideration was investigated in detail in [35]. For a Gaussian beam, the IFS can be deduced from the complex reflection coefficients $\mathfrak{R}_s$

and $\mathfrak{R}_p$ as [6]:

$$\Delta T = -\frac{a_p a_s \cot\theta}{k_0(R_s^2 a_s^2 + R_p^2 a_p^2)}[(R_p^2 + R_s^2)\sin\delta + 2\,R_p\,R_s\sin(\delta + \psi_s - \psi_p)], \quad (8)$$

where $\mathfrak{R}_{p,s} = R_{p,s}\exp(\mathrm{i}\,\psi_{p,s})$, and $a_{p,s} \in \mathbb{R}^+$ and δ are related to the normalized electric field (or Jones vector) of the incident beam defined as $\mathbf{e} = a_p\,\hat{\boldsymbol{x}} + a_s\exp(\mathrm{i}\delta)\hat{\boldsymbol{y}}$, with $a_p^2 + a_s^2 = 1$. Note that equation (8) is not valid at normal incidence (where the value of the IFS diverges towards infinity), where the notions of *s* and *p* polarizations, as well as the distinction between GHS in the plane of incidence and IFS perpendicular to that plane, become irrelevant.

As evidenced by equations (7)–(8), strain-induced changes of $\mathfrak{R}_{s,p}$ are thus bound to exert an influence on both δ_{TMOKE} and ΔT, as will be demonstrated in the next section.

3. Numerical results and discussion

In this section, we illustrate the theoretical calculations detailed above using the parameters for YIG and GGG gathered in table 1 of [35]. At the chosen near-infrared wavelength $\lambda_0 = 1.15\,\mu$m, absorption in both materials can be neglected. Unless otherwise specified, all calculations are performed for magnetization in the magnetic film saturated in the positive direction parallel to the *y*-axis, i.e., for $m_y = +1$.

As in our previous study [35], the thicknesses of the YIG and GGG layers are taken as integer multiples of d_1 and d_2, respectively defined so that both layers are of equal half-wave optical thickness [43]:

$$d_1\sqrt{\varepsilon_1 - \sin^2\theta_{\mathrm{HW}}} = d_2\sqrt{\varepsilon_2 - \sin^2\theta_{\mathrm{HW}}} = \lambda_0/2, \quad (9)$$

where θ_{HW} is the incidence angle satisfying the half-wave condition. This choice is made in order to emphasize the effect of strain for incidence conditions where reflection and spatial shift are nearly zero in an unstrained structure. In the following, calculations are performed for the incidence angle satisfying the half-wave condition at $\theta_{\mathrm{HW}} = 10°$ with $d_1 = 0.270\,\mu$m and $d_2 = 0.298\,\mu$m.

An estimate of the critical thickness of the pseudomorphic layer in each material is $h_c^{(1)} \approx h_c^{(2)} \approx 0.1\,\mu$m [35].

3.1. Influence of strain on reflection coefficients and TMOKE

In this subsection, the influence of strain and magnetization reversal on the reflections coefficients of the eigenmodes and on TMOKE is studied.

The angular variations of the moduli R_s and R_p of complex reflection coefficients $\mathfrak{R}_s$ and $\mathfrak{R}_p$ in the vicinity of θ_{HW} are presented in figure 2(a). The reflection coefficients $R_{s,p}^{(0)}$ of the unstrained structure (solid lines) are compared to its reflection coefficients $R_{s,p}$ (dashed lines) when strain at the YIG/GGG interface is taken into account. In the unstrained system, both $R_s^{(0)}$ and $R_p^{(0)}$ turn to zero at precisely θ_{HW}. The minima of R_s and R_p in the presence of strain are no longer zero, slightly differ from each other, and their angular positions are shifted with respect to θ_{HW} towards larger (respectively, smaller) angles for R_s (respectively, R_p). This reflects the anisotropy of the strained system, where R_s is related to the component of the incoming optical field along the *y*-axis (thus, parallel to the interfaces), while the behavior of R_p is affected by the inhomogeneity of the structure along the *z*-axis. Similarly, while $R_s^{(0)}$ and $R_p^{(0)}$ are almost equal in the vicinity of θ_{HW}, strain lifts that degeneracy, with $R_s > R_p$ below a crossing point at $\theta \approx \theta_{\mathrm{HW}}$ and $R_s < R_p$ above that point. These features will help understand the variations of the IFS around θ_{HW} in section 3.2.

The effect of a magnetization reversal in the YIG film is shown in figure 2(b). As the magnetic gyrotropy of the YIG layer was neglected, δ_{TMOKE} assumes non-zero values for *p*-polarized light only, as only $\mathfrak{R}_p$ depends on the off-diagonal elements of the permittivity tensor of the magnetic medium (see equation (3)). Figure 2(b) compares the angular dependence of δ_{TMOKE} for a linearly *p*-polarized incident beam when strain at the YIG/GGG interface is neglected (blue solid line) and when it is taken into account (red dashed line). A peak of TMOKE parameter δ_{TMOKE} can be observed in both cases near $\theta = \theta_{\mathrm{B}} = 63.75°$. This angle corresponds to the pseudo-Brewster condition for the bilayer, i.e., the angle at which the reflectivity of the bilayer reaches a near-zero minimum for *p*-polarized light. As can be seen from figure 2(b), strain only induces a slight increase and narrowing of that peak. More noticeable is the appearance of a very narrow peak of δ_{TMOKE} in the vicinity of the half-wave angle $\theta_{\mathrm{HW}} = 10°$, where the TMOKE parameter is almost zero when no strain is present in the system. With strain, δ_{TMOKE} experiences a rapid change of sign at an angle close to θ_{HW}, where $I^{(r)}(m_y = +1) = I^{(r)}(m_y = -1) = I^{(r)}(m_y = 0)$, which means that at that angle, the strain-induced contribution to TMOKE is compensated by its magnetization-dependent contribution. In any case, both TMOKE peaks correspond to small values of the reflectivity. It should be noted, however, that the typical experimental sensitivity of TMOKE measurements ($\sim 10^{-3}$) allows the detection of such variations of δ_{TMOKE} [44].

For incident states of polarization other than the linear *p*-polarized state, TMOKE does not produce any effect in first approximation, but a noticeable Imbert–Fedorov effect can nevertheless take place. In the following, we concentrate on the dependences of the IFS upon the incident state of polarization, a reversal of the magnetization in the YIG layer, and the thicknesses of the layers (while retaining the half-wave condition).

3.2. Influence of light polarization on the strain-induced IFS

As is well known, an incident beam linearly polarized along the *s* or *p* directions does not yield any transverse IFS. This corresponds in equation (8) to $a_p = 0$ and $a_s = 0$, respectively. In all other cases, the amplitude and sign of the shift depend in an intricate way on the shape of the polarization ellipse and its helicity.

In figure 3, we study the angular dependence of the reduced IFS $\Delta Y = \Delta T/\lambda_0$ for various ellipticities of the

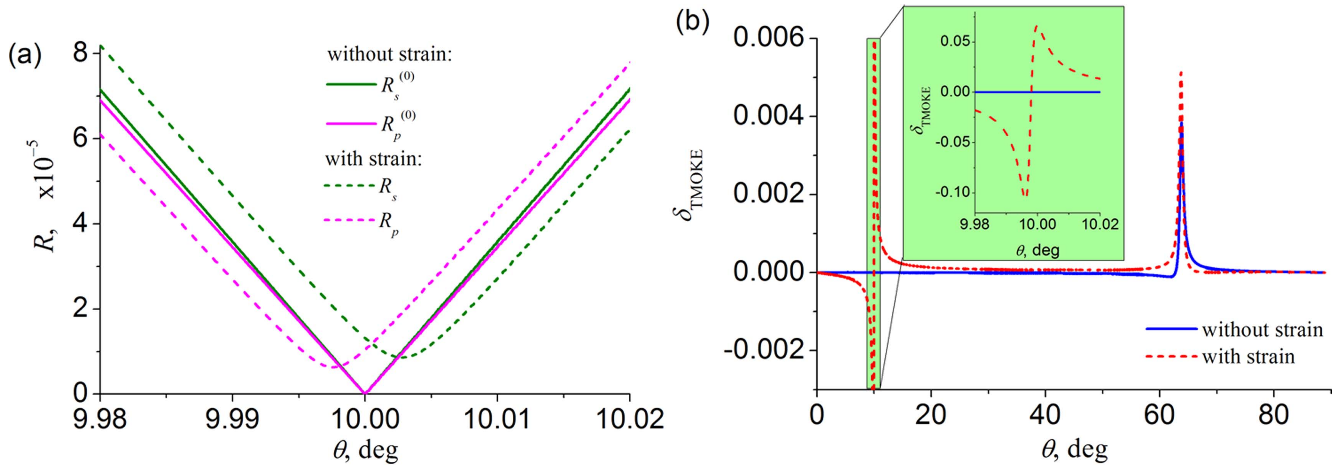

Figure 2. (a) Moduli of reflection coefficients $\Re_s$ and $\Re_p$ as functions of the incidence angle θ in the vicinity of θ_{HW} (green and magenta lines, respectively). (b) TMOKE parameter δ_{TMOKE} as a function of θ for a p-polarized incident wave. Solid and dashed lines refer to the unstrained and strained systems, respectively.

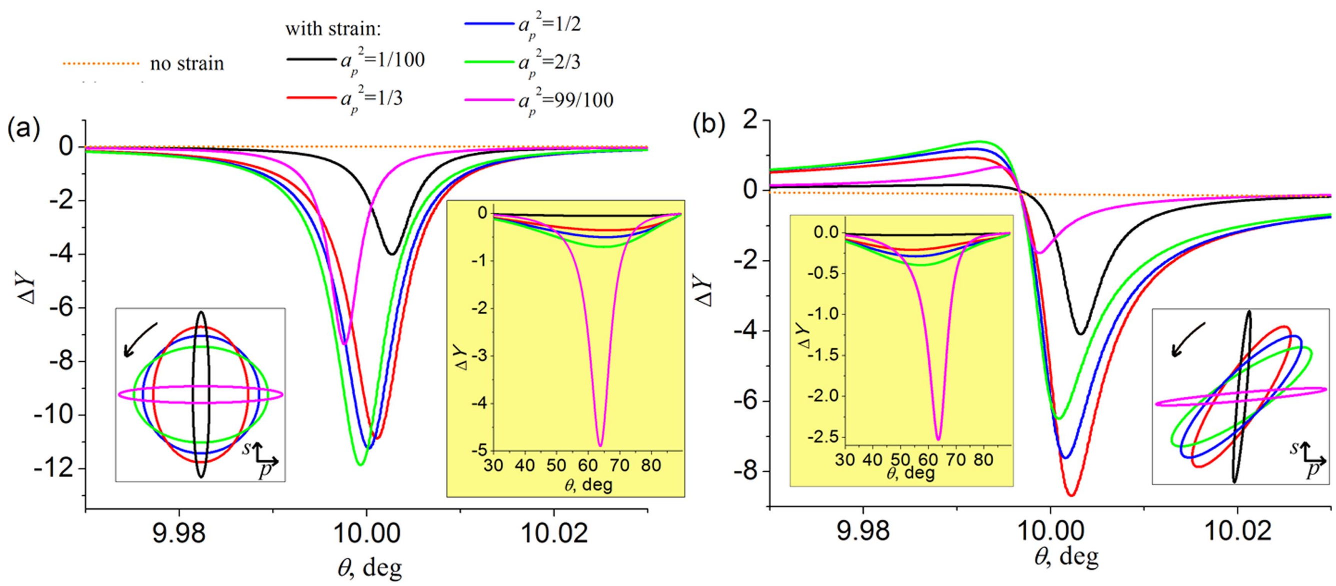

Figure 3. Reduced IFS amplitude $\Delta Y = \Delta T/\lambda_0$ of the elliptically-polarized incident beam as a function of the angle of incidence θ in the vicinity of θ_{HW} (inset: at large θ) for (a) $\delta = \pi/2$ and (b) $\delta = \pi/6$. The dotted orange line represents the transverse shift without taking YIG/GGG interfacial strain into account. The solid lines show the shift for different states of ellipticity of the incident light when strain is accounted for. The shape and helicity of the incident polarization ellipse are indicated in the s and p system of axes for any given angle of incidence.

incident state of polarization and in two cases of left-handed elliptically-polarized incident beams: when the axes of the incident ellipse of polarization are parallel to the s and p directions ($\delta = \pi/2$, figure 3(a)) and when they are rotated with respect to these directions (here for $\delta = \pi/6$, figure 3(b)). The shape of the polarization ellipse of the incident beam and helicity are indicated as a visual aid to the discussion of the simulation results. In each case, the dotted orange line represents the transverse shift without YIG/GGG interfacial strain, while the solid lines show its variations when strain is taken into account for various states of ellipticity of the incident light.

The impact of strain on the IFS appears to be significant near θ_{HW}, where both s and p reflection coefficients $\Re^{(0)}_{s,p}$ reach zero in the unstrained structure. As previously noted, the near-zero minima of $\Re_s$ and $\Re_p$ appear at slightly different angles near θ_{HW} due to the anisotropy of strain in the structure. For $\delta = \pi/2$, the IFS exhibits a pronounced negative peak (with an amplitude of several λ_0) around this incidence angle when strain is taken into account (solid curves in figure 3), whereas ΔY does not exceed about $10^{-3}\ \lambda_0$ when strain is neglected (dotted line). Starting from the limiting case of an s-polarized beam ($a_p = 0$) for which $\Delta Y = 0$, a non-zero p-polarized contribution to the incident wave (i.e., a non-zero value of a_p) produces a peak of IFS. With an increase of a_p, the position of that peak drifts towards smaller incidence angles and the peak values of ΔY increase (black, red, blue and green lines in figure 3(a) for $a_p^2 = 1/100$, $1/3$, $1/2$, and $2/3$, respectively) until the p-polarized fraction of the incident light (in terms of intensity) reaches about 90%, after which ΔY decreases (see for instance the magenta line in figure 3(a) for $a_p^2 = 99/100$) towards zero when the other limiting case of a p-polarized linear incident polarization is reached ($a_s = 0$). The position of the minimum of ΔY for a circularly-polarized incident beam (blue line, $a_p^2 = 1/2$) corresponds to the angle at which $R_s = R_p$ in figure 2(a). The shift of that minimum towards smaller (respectively, larger) incidence angles for $a_p^2 = 2/3$ (respectively, $a_p^2 = 1/3$) reflects the domination of either the p- or the s-component of the incident field in each case (as illustrated by the corresponding polarization ellipses) and thus can be related to the respective angular positions of the minima of R_s and R_p discussed in section 3.1.

The IFS also possesses a negative maximum (depending on the shape of the incident polarization ellipse, it varies from a few tenths of λ_0 to a few λ_0) in a broad angular region around the pseudo-Brewster angle θ_{B} where the reflectivity of the sole p-polarized component approaches zero [35]. The amplitude of the peak of ΔY increases in absolute value with the fraction of p-polarized incoming light and reaches a maximum for $a_p = 1$ (see solid lines in the inset of figure 3(a)). It should be noted that, except in the vicinity of θ_{HW}, the impact of strain on the IFS is negligible, and the dotted line coincides with the solid line for any given state of incoming polarization.

It should be noted that, for any state of incident polarization, the transverse IFS in the vicinity of θ_{B} is one order of magnitude smaller than the corresponding lateral GHS [35]. Moreover, the lateral GHS $\Delta X = \Delta L/\lambda_0$ is caused by an abrupt change of the phase of the reflected light, which takes place in a much narrower region surrounding θ_{B} than the decrease of $\mathfrak{R}_p$ that mostly governs the IFS near that angle of incidence. Thus the peak of ΔY is broader than that of ΔX in the same YIG/GGG bilayer [35]. Furthermore, the contribution of strain to the IFS around θ_{B} lies within the range $(10^{-5} \div 10^{-3})\lambda_0$, which is between 1 and 3 orders of magnitude less than its contribution to the GHS [35]. It must also be noted that, contrary to the GHS, whose absolute value increases when the incoming beam tends towards grazing incidence, the IFS decreases down to zero at incidence angles close to 90°.

The tendencies observed for $\delta = \pi/2$ remain qualitatively true for $\delta = \pi/6$. The position of the peak of IFS when a_p increases follows the same behavior, but its value for $a_p^2 = 1/2$ (blue line, with an equal weight of the s and p components of the incident wave but no longer a circular polarization) does not correspond anymore to the angle at which $R_s = R_p$ in figure 2(a). However, as mentioned earlier, a rotation of the axes of the polarization ellipse (related to the value of δ) is likely to lead to significant quantitative changes to the amplitude of the transverse shift and even to its sign. This is illustrated in figure 3(b), where it can be seen that for $\delta = \pi/6$ the reduced shift ΔY assumes positive values for small incidence angles and changes sign in the vicinity of θ_{HW}. The negative peak amplitudes of ΔY for $a_p^2 = 1/100$ and $1/3$ are larger in absolute value than those obtained for $\delta = \pi/2$ (see black and red solid lines in figures 3(a) and (b)), and the opposite observation can be made for $a_p^2 = 1/2$, $2/3$, and $99/100$ (see blue, green, and magenta solid lines). A more detailed study shows that the peak value of ΔY actually reaches a maximum of more than 8 λ_0 for a p-polarized fraction of the incident light (in terms of intensity) of about 35%. The same tendency can be observed for the positive peaks of ΔY (for $\theta < \theta_{\mathrm{HW}}$), whose value does not exceed 1.5 λ_0.

For a given ratio of p-component in the incident beam, its state of polarization, i.e., the shape as well as the helicity of its characteristic polarization ellipse, noticeably influence the angular position, magnitude, and sign of the peak of IFS around θ_{HW}. This is illustrated in figure 4 where the angular dependence of ΔY in the vicinity of θ_{HW} is shown for various left-handed incident states of polarization, when the phase difference δ between the p and s components verifies (I) $0 \leqslant \delta \leqslant \pi/2$ and (II) $\pi/2 \leqslant \delta \leqslant \pi$, and right-handed incident states of polarization, for (III) $-\pi \leqslant \delta \leqslant -\pi/2$ and (IV) $-\pi/2 \leqslant \delta \leqslant 0$. In all cases, $a_p = a_s = 1/\sqrt{2}$. The results gathered in figure 4 confirm the importance of both the ellipticity (i.e., shape) and helicity of the polarization ellipse on the IFS amplitude and sign. In the particular set of incident states of polarization given by the condition $a_p = a_s = 1/\sqrt{2}$, one notices that for a given ellipticity, reversing the helicity (i.e., replacing δ with $-\delta$) induces a *non-reciprocal* (in terms of the absolute value of the IFS amplitude and angular position of the IFS peak) reversal of sign of the shift, as attested by a comparison of quadrants (I) and (IV), or (II) and (III). Moreover, a 90° rotation of the polarization ellipse does not affect the sign of the IFS but yields both an angular drift of the IFS peak (towards smaller incidence angles) and a slight change of its amplitude, as can be seen by comparing quadrants (I) and (II), or (III) and (IV). Furthermore, such a 90° rotation of the ellipse ($\delta \to \delta + \pi/2$) and an inversion of its helicity yields a *reciprocal* inversion of the IFS peak (same angular position, inverted sign), as evidenced by a comparison between quadrants (I) and (III), or (II) and (IV), of figure 4. Finally, let us note that, as previously mentioned, incident light linearly polarized in a direction other than the s and p axes, does yield an IFS, as shown by the results obtained for $\delta = 0$ and $\delta = \pi$ (black lines), which correspond to an incident beam linearly polarized at ±45° from the s and p directions for any given angle of incidence. Similar observations could be made for any ration between a_s and a_p.

3.3. Influence of a magnetization reversal on the strain-induced IFS

The magnetic anisotropy in the magnetic film is also expected to have an impact on the IFS experienced by incoming light. In this subsection, the IFS is respectively denoted $\Delta Y^{(+1)}$ and $\Delta Y^{(-1)}$ when the magnetic film is magnetized to saturation parallel ($m_y = +1$) and antiparallel ($m_y = -1$) to unit vector $\hat{\boldsymbol{y}}$, and $\Delta Y^{(0)}$ when the film is demagnetized ($m_y = 0$).

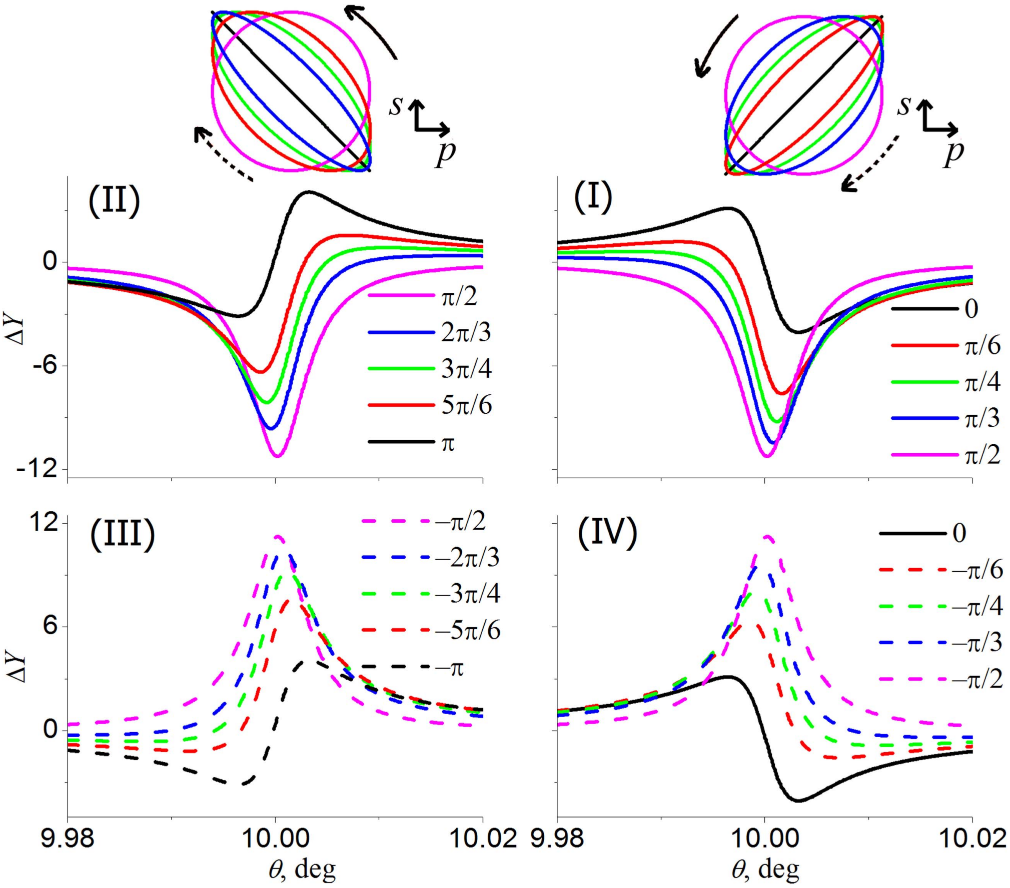

Figure 4. Reduced IFS amplitude $\Delta Y = \Delta T/\lambda_0$ as a function of the angle of incidence θ in the vicinity of θ_{HW} of an elliptically-polarized incident beam (with $a_p = a_s = 1/\sqrt{2}$) reflected from the strained structure for different values of the phase difference δ between the s and p components of left-handed elliptically polarized light: (I) $0 \leqslant \delta \leqslant \pi/2$ and (II) $\pi/2 \leqslant \delta \leqslant \pi$; and of left-handed elliptically polarized light: (III) $-\pi \leqslant \delta \leqslant -\pi/2$ and (IV) $-\pi/2 \leqslant \delta \leqslant 0$. The shape and helicity of the incident polarization ellipse are indicated in the s and p system of axes for any given angle of incidence.

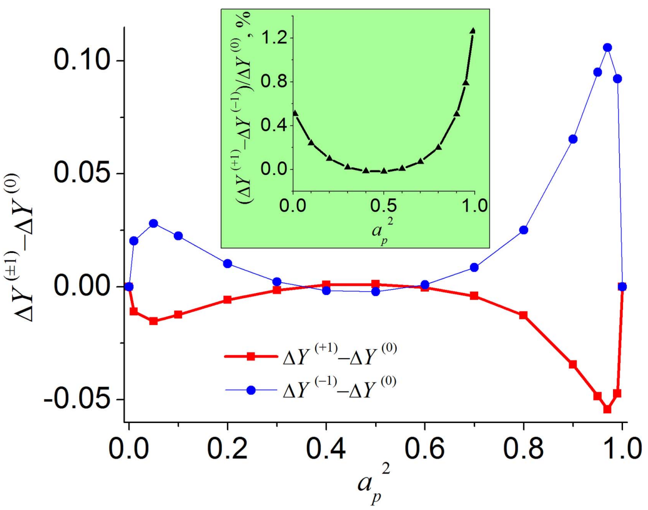

Figure 5. Evolution with $a_p^2$of the absolute differences in reduced IFS $\Delta Y^{(+1)} - \Delta Y^{(0)}$ (red line) and $\Delta Y^{(-1)} - \Delta Y^{(0)}$ (blue line). The inset shows the relative difference $(\Delta Y^{(+1)} - \Delta Y^{(-1)})/\Delta Y^{(0)}$. Calculations are performed for $\delta = \pi/2$ and at incidence angles (for each value of a_p^2) for which the corresponding IFS is maximal.

Figure 5 presents the dependence, as functions of a_p^2, of the absolute reduced IFS differences $\Delta Y^{(+1)} - \Delta Y^{(0)}$ (red line) and $\Delta Y^{(-1)} - \Delta Y^{(0)}$ (blue line). As is the case for the amplitude and position of IFS peaks, the impact of magnetization reversal on the IFS strongly depends on the state of polarization of the incident beam. Here the axes of the polarization ellipse are chosen to coincide with the s and p directions ($\delta = \pi/2$). For each value of a_p^2, the angle of incidence is that for which the values of $\Delta Y^{(+1)}$, $\Delta Y^{(-1)}$, and $\Delta Y^{(0)}$ are all maximal (all three shifts reach their maximum at the same angle of incidence, regardless of the magnetization, and this angle is, as illustrated by figures 3 and 4, always in the vicinity of θ_{HW}).

Upon magnetization reversal, the off-diagonal components of the permittivity tensor (equation (3)) change sign, which explains the opposite signs of the absolute differences $\Delta Y^{(+1)} - \Delta Y^{(0)}$ (red line) and $\Delta Y^{(-1)} - \Delta Y^{(0)}$ (blue line). The effect of the magnetization of the magnetic film on the IFS difference is noticeable, but remains small and furthermore, it is not reciprocal upon magnetization reversal, although the general shape of both shift differences is the same. Between the limiting cases of a linearly s- or p-polarized light ($a_p^2 = 0$ and $a_p^2 = 1$, respectively) for which no IFS can be observed,

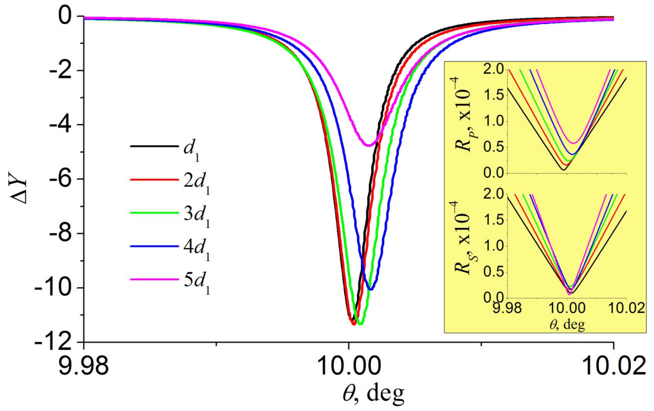

Figure 6. Reduced IFS amplitude ΔY of circularly polarized incident light as a function of the angle of incidence θ in the vicinity of θ_{HW} for increasing values of the magnetic YIG film thickness D_1. Here the GGG slab thickness is set to $D_2 = 4 \times d_2$. The inset shows the corresponding angular evolution of reflectivities R_s and R_p in each case.

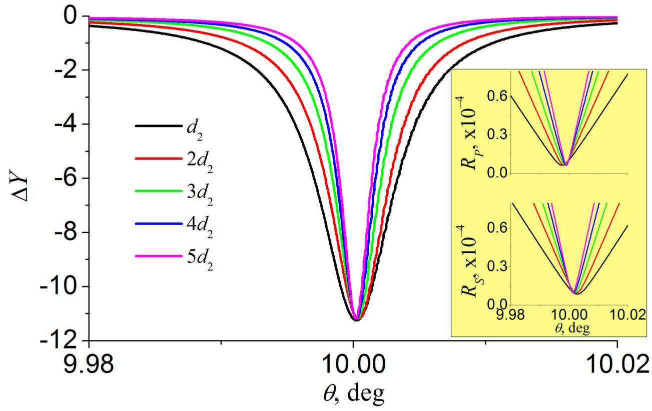

Figure 7. Reduced IFS amplitude ΔY of circularly polarized incident light as a function of the angle of incidence θ in the vicinity of θ_{HW} for increasing values of the GGG slab thickness D_2. Here the YIG film thickness is set to $D_1 = d_1$. The inset shows the corresponding angular evolution of reflectivities R_s and R_p in each case.

figure 5 shows that the amount of p-polarized light in the incident beam governs the impact of a magnetization reversal on the amplitude of the IFS. As previously stated, this stems from the fact that when the magnetic gyrotropy of the YIG film is neglected, only $\mathfrak{R}_p$ depends on m_y. With this choice of incoming polarization, the IFS is negative for all values of magnetization. However, magnetizing the film parallel to $\hat{\boldsymbol{y}}$ ($m_y = +1$) results in a slight increase of IFS in absolute value (up to approximately 5% of of λ_0), while magnetizing it antiparallel to $\hat{\boldsymbol{y}}$ ($m_y = -1$) induces a somewhat larger reduction of IFS in absolute value (up to 10% of λ_0). For the value of δ chosen in figure 5, the impact of a magnetization reversal is in both cases highest for $a_p \approx 90\%$ and almost zero for a circularly-polarized incident wave ($a_p^2 = 0.5$). The inset shows the relative difference $(\Delta Y^{(+1)} - \Delta Y^{(-1)})/\Delta Y^{(0)}$ and highlights this tendency. The results shown in figures 3 and 4, however, make it clear that both the value of a_p for which the magnetically-induced variations of the IFS are highest, and the magnitudes of those variations, would be different for other choices of δ.

Finally, it must be noted that the absolute variation of the transverse IFS ΔY upon magnetization reversal is of the same order of magnitude as that of the corresponding variation of the lateral GHS in the same bilayer [35].

3.4. Influence of the film thicknesses on the strain-induced IFS

As evidenced by equation (8), the value of the IFS is directly related to the overall complex reflectivity factors $\mathfrak{R}_s$ and $\mathfrak{R}_p$ of the bilayer. As such, it depends on the interference between waves transmitted and reflected at all three interfaces of the system, and thus must depend on the thicknesses D_1 and D_2 of the YIG and GGG films constituting the bilayer (figure 1). In the following, the magnetic film is magnetized at saturation parallel to unit vector $\hat{\boldsymbol{y}}$, and D_1 and D_2 are integer multiples of the nominal thicknesses d_1 and d_2 defined in equation (14) in order to preserve the half-wave condition.

The angular dependences, in the vicinity of θ_{HW}, of the reduced transverse shift ΔY are shown in figure 6 for different values of the YIG slab thickness D_1 in the case of a circularly-polarized incident beam ($a_p = a_s = 1/\sqrt{2}$ and $\delta = \pi/2$). The GGG slab thickness is set to $D_2 = 4 \times d_2$ in order to keep it comparable to D_1 in all cases. As was previously established, the value, and particularly the position, of the IFS near θ_{HW} is closely related to the variations of the reflectivities R_s and R_p in the same range (see inset). As seen in section 3.1 and figure 2, both reflectivities exhibit a dip in the vicinity of θ_{HW}.

The simulation results indicate that an increase of the magnetic film thickness D_1 leads to an overall decrease (in absolute value) of the strain-induced IFS peak, while its angular position drifts towards larger incidence angles, and its full width at half maximum increases. Comparing these tendencies with the variations of R_s and R_p leads to interpret them in terms of a combined, as well as competing, influence of these reflectivities: away from θ_{HW}, the domination of R_p over R_s gives it a prevalent role in the overall behavior of the IFS, which thus follows both the drift towards larger incidence angles and the decrease of the minimum of R_p in the vicinity of θ_{HW}. Moreover, as D_1 increases, the angular range over which the values of R_s and R_p are comparable also increases, and their combined influence tends to justify the broadening of the IFS peak.

In comparison, it should be noted that the corresponding GHS dependence upon thickness D_1 in the same bilayer exhibits a very different, and non-monotonous, behavior for both s- and p-polarized incident light [35].

A similar study can be made for the influence of the thickness D_2 of the GGG layer. Figure 7 presents the angular dependences, over the same angular range in the vicinity of θ_{HW}, of the reduced transverse shift ΔY for different values of D_2, again in the case of a circularly-polarized incident beam. The YIG film thickness is set to $D_2 = d_1$. As in figure 6, the variations of reflectivities R_s and R_p in the same range are shown in the inset.

In this case, the simulation indicates a markedly different influence of the thickness D_2 of the GGG layer. An increase of D_2 virtually affects neither the amplitude of the strain-induced IFS peak nor its angular position (which remains very close to θ_{HW}). Only the full width at half maximum of that peak shows any noticeable influence of D_2, as it narrows when the GGG layer thickness increases. Again, the variations of R_s and R_p help to interpret the simulation results. Contrary to the previous case, these variations are here very similar for a given value of D_2, both in terms of amplitude and angular dependence in the vicinity of θ_{HW}. Thus neither of these reflectivities dominates. Rather, their influences reinforce one another. Indeed, as neither R_s nor R_p exhibits any noticeable angular drift or variation of its minimum value at θ_{HW} when D_2 increases, so do the peak amplitude and angular position of ΔY remain virtually unchanged. Moreover, for a given value of D_2, the values of R_s and R_p as functions of θ are almost identical. As a result, the variation of the angular width of the ΔY peak closely follows that of R_s and R_p, which explains that its full width at half maximum evolves like those of the reflectivity dips shown in the inset, i.e., narrows as D_2 increases.

Again, comparing these results with those obtained for the GHS in the same system shows a very different behavior, as the amplitude of the GHS increases with GGG layer thickness D_2 [35]. More precisely, as D_2 increases, so do the derivatives of phases ψ_s and ψ_p with respect to θ (which follow the same dependence upon thickness D_2 as that of moduli R_s and R_p shown in the inset of figure 7), and so does the GHS. In contrast to that behavior, the amplitude of the IFS does not vary with thickness D_2.

4. Conclusions

We have theoretically studied the influence of misfit strain on the TMOKE and the transverse Imbert–Fedorov beam shift that can be expected upon reflection of an elliptically-polarized electromagnetic wave on the upper surface of a bilayer consisting of a magnetic YIG film epitaxially grown on a non-magnetic GGG slab.

We have shown that the mechanical strain near the geometrical YIG/GGG interface can enhance both the the IFS and the TMOKE. The latter, that can only be observed for a p-polarized incident beam, has been demonstrated to be notably enhanced by strain when the half-wave condition is satisfied, as well as, to a lesser extent, near pseudo-Brewster incidence. The IFS has also been shown to strongly increase with strain if the angle of incidence is close to satisfying the half-wave condition for both layers, with a peak value that can reach up to about ten incident light wavelengths.

As a rule, the amplitude and sign of the peak of IFS have been demonstrated to be largely governed by the polarization state of the incident wave, in terms of ellipticity, tilt of the polarization ellipse, and helicity.

Furthermore, the relative variation of the IFS upon a magnetization reversal in the YIG film has been estimated to be of the order of 1% (thus much smaller than the corresponding variation of the GHS previously studied in the same system), whether or not strain is present at the YIG/GGG interface. Overall, both the strain-induced IFS observed for the half-wave condition and the shift at pseudo-Brewster incidence have been found to be one order of magnitude smaller than the GHSs previously studied in the same system [35].

Finally, an increase of the YIG film thickness has been shown to reduce the amplitude of the strain-induced peak of IFS, and an increase of the GGG slab thickness to narrow the angular width of that peak.

These results point to possible ways to control (enhance or reduce) the Imbert–Fedorov transverse shift experienced by a light beam upon reflection on a YIG-GGG bilayer in MO devices, essentially through the choice of the angle of incidence and/or state of polarization of the beam, and, to some degree, through the direction of the magnetization in the YIG layer.

Acknowledgments

This work was partly supported by: European Union's Horizon 2020 Research and Innovation Programme (grant No. 644348), MPNS COST Action (project No. MP1403), École Nationale d'Ingénieurs de Brest (grant No. 14MOES-MOMO14), the Ministry of Education and Science of the Russian Federation (projects No. 14.Z50.31.0015 and No. 3.2202.2014/K), and the Ukrainian State Fund for Fundamental Research (project No. Φ71/73-2016).

References

[1] Goos F and Hänchen H 1947 *Ann. Der Phys.* **1** 333
[2] Fedorov F I 1955 *Dokl. Akad. Nauk SSSR* **105** 465 (in Russian)
[3] Imbert C 1972 *Phys. Rev.* D **5** 787
[4] Pillon F, Gilles H and Girard S 2004 *Appl. Opt.* **43** 1863
[5] Bliokh K Y and Aiello A 2013 *J. Opt.* **15** 014001
[6] Aiello A and Woerdman J P 2008 *Opt. Lett.* **33** 1437
[7] Goswami S, Dhara S, Pal M, Nandi A, Panigrahi P K and Ghosh N 2016 *Opt. Express* **24** 6041
[8] Götte J B and Dennis M R 2013 *Opt. Lett.* **38** 2295
[9] Swain P K, Goswami N and Saha A 2017 *Opt. Commun.* **382** 1
[10] Ornigotti M and Aiello A 2013 *J. Opt.* **15** 014004
[11] Merano M, Aiello A, 't Hooft G W, von Exter M P, Elier E R and Woerdman J P 2007 *Opt. Express* **15** 15928
[12] Goswami Kar N and Saha A 2014 *Opt. Commun.* **330** 169
[13] Fan Y, Shen N-H, Zhang F, Wei Z, Li H, Zhao Q, Fu Q, Zhang P, Koschny T and Soukoulis C M 2016 *Adv. Opt. Mater.* **4** 1824
[14] Borisov S B, Dadoenkova N N, Lyubchanskii I L and Lyubchanskii M I 1998 *Opt. Spectrosc.* **85** 225
[15] Tang T, Qin J, Xie J, Deng L and Bi L 2014 *Opt. Express.* **22** 27042
[16] Cheng M, Fu P, Weng M, Chen X, Zeng X, Feng S and Chen R 2015 *J. Phys. D: Appl. Phys.* **48** 285105
[17] Dadoenkova Y S, Dadoenkova N N, Lyubchanskii I L and Lee Y P 2015 *J. Appl. Phys.* **118** 213101
[18] Soboleva I V, Moskalenko V V and Fedyanin A A 2012 *Phys. Rev. Lett.* **108** 123901

[19] Dadoenkova Y S, Dadoenkova N N, Lyubchanskii I L, Lee Y P and Rasing T 2013 *Photon. Nanostruct. Fundam. Appl.* **11** 345
[20] Liu F, Xu J, Song G and Yang Y 2013 *J. Opt. Soc. Am.* B **30** 1167
[21] Xu G, Xiao Y, Li J, Mao H, Sun J and Pan T 2013 *Ann. Phys., NY* **335** 33
[22] Grosche S, Ornigotti M and Szameit A 2015 *Opt. Express* **23** 30195
[23] Tang T, Luo L, Liu W, He X and Zhang Y 2015 *Appl. Phys.* B **180** 497
[24] Tang T, Li C, Luo L, Zhang Y and Yuan Q 2016 *Opt. Commun.* **370** 49
[25] Jiang Q D, Jiang H, Liu H, Sun Q F and Xie X C 2015 *Phys. Rev. Lett.* **115** 156602
[26] Asiri S, Xu J, Al-Amri M and Suhail Zubairy M 2016 *Phys. Rev.* A **93** 013821
[27] Borhanian J 2015 *Phys. Plasmas* **22** 032108
[28] Jain S C, Harker A H and Cowley R A 1997 *Phil. Mag.* A **75** 1461
[29] Howe J M 1997 *Interfaces in Materials* (Hoboken, NJ: Wiley)
[30] Lyubchanskii I L, Dadoenkova N N, Lyubchanskii M I, Rasing T, Jeong J W and Shin S C 2000 *Appl. Phys. Lett.* **76** 1848
[31] Lyubchanskii I L, Jeong J W, Shin S C, Dadoenkova N N, Lyubchanskii M I and Rasing T 2000 *J. Appl. Phys.* **87** 6794
[32] Jeong J W, Shin S C, Lyubchanskii I L and Varyukhin V N 2000 *Phys. Rev.* B **62** 13455
[33] Zabolotin A E, Dadoenkova N N, Bentivegna F F L, Lyubchanskii I L, Shyshmakov A L, Lee Y P, Boucher Y G and Rasing T 2011 *J. Opt. Soc. Am.* B **28** 2216
[34] Sánchez A and Orozco S 2016 *J. Opt. Soc. Am.* B **33** 1406
[35] Dadoenkova Y S, Bentivegna F F L, Dadoenkova N N, Lyubchanskii I L and Lee Y P 2016 *J. Opt. Soc. Am.* B **33** 393
[36] Zvezdin A K and Kotov V A 1997 *Modern Magnetooptics and Magnetooptical Materials* (Bristol: Institute of Physics)
[37] Zhang Q, Li Y, Nurmikko A V, Miao G X, Xiao G and Gupta A 2004 *J. Appl. Phys.* **96** 7527
[38] Valvidares S M, Schroeder T, Robach O, Quirós C, Lee T L and Ferrer S 2004 *Phys. Rev.* B **70** 224413
[39] Arregi J A, González-Díaz J B, Idigoras O and Berger A 2015 *Phys. Rev.* B **92** 184405
[40] Martinez J C, Jalil M B A and Tan S G 2012 *Opt. Lett.* **37** 3237
[41] Winkler G 1981 *Magnetic Garnets* (Braunschweig: Vieweg)
[42] Borisova S D and Naumov I I 1999 *Russ. Phys. J.* **42** 420
[43] Born M and Wolf E 1959 *Principles of Optics* (London: Pergamon)
[44] Belotelov V I, Akimov I A, Pohl M, Kotov V A, Kasture S, Vengurlekar A S, Venu G A, Yakovlev D R, Zvezdin A K and Bayer M 2011 *Nat. Nanotechnol.* **6** 370